Supporting Information

Bristow et al. 10.1073/pnas.0901080106

SI Text

Lithological Description of the Doushantuo Formation in Yangtze Gorges. Member 1 consists of the cap carbonate, typically 3 to 5 m thick and in sharp lithological contact with underlying glacial diamictite of the Nantuo Formation (1). Member 2 is ≈70 m thick and consists of calcareous mudstones and marls alternating with parallel-laminated limestone and dolomite beds at scales of a few centimeters to several meters. Argillaceous member 2 gradually changes to carbonate-dominated member 3 that is characterized by cm-scale alternating limestone/dolostone ribbon rock and is approximately 70 m in thickness. Approximately 10 m of organic-rich shales of member 4 contain decimeter-scale oval limestone concretions and form a sharp lithological contact with the underlying ribbon rock. Ash layers, dated as 635.2 ± 0.6 Ma and 632.5 ± 0.5 Ma occur within the cap carbonate and approximately 5 m above the cap. A third ash, at the top of the formation, is dated as 551.7 ± 0.7 Ma (2).

Background Information on Mg-Clays. Saponite is a trioctahedral smectite and from a geochemical perspective is part of a group of Mg-rich clays that also includes palygorskite, sepiolite, and stevensite. These minerals are compositionally and texturally distinctive and reflect different formation mechanisms under different chemical conditions. Stevensite and sepiolite contain little or no aluminum and often form by direct precipitation (3–6). In contrast, palygorskite and saponite contain significant amounts of structural aluminum, indicating formation via transformation of precursor Al-bearing clay (7). Topotatic overgrowth of stevensitic layers on preexisting phyllosilicate sheets has been proposed as the transformation mechanism resulting in Mg-smectites with saponitic compositions (8). Palygorskite and sepiolite have chain structures and are readily distinguished from sheet-like stevensite and saponite XRD analysis and by their fibrous fabrics.

In subaqueous sedimentary settings the type of Mg-clay forming is governed by chemical conditions and the availability of detrital Al-silicates. In Phanerozoic sedimentary deposits, fibrous clays like palygorskite and sepiolite tend to form at moderate pH (~8) and are found in peri-marine basins (3) and high-stand sediments of closed lake systems (9, 10). Thermodynamic calculations indicate that fibrous clays are favored by high silica activities (11), but as pointed out in the main text, kinetic controls are critical. Stevensite and saponite are more prevalent under high pH (~9 or more) and/or evaporative conditions in which Mg is concentrated by a factor of 10 (see Table S5). However, it should be pointed out that the assemblages of Mg-clay minerals are not mutually exclusive and commonly occur together.

The random fabrics of clay floccules commonly observed in samples of the Doushantuo Formation, combined with compositional information showing appreciable Al content (Table S1), suggest that most saponite formed by transformation of detrital precursors. Given the high degree of illitization of clays in ash beds and chloritization of saponite in some parts of sections, the absence of other types of Mg-clays may be a result of greater susceptibility to diagenetic alteration.

1. Jiang G, Kennedy MJ, Christie-Blick N (2003) Stable isotopic evidence for methane seeps in Neoproterozoic postglacial cap carbonates. *Nature* 426:822–826.
2. Condon D, et al. (2005) U-Pb ages from the Neoproterozoic Doushantuo Formation, China. *Science* 308:95–98.
3. Weaver CE, Beck KC (1977) in *Miocene of the SE United States: A Model for Chemical Sedimentation in a Peri-marine Environment* (Amsterdam, Elsevier).
4. Tettenhorst R, Moore GE, Jr (1978) Stevensite oolites from the Green River Formation of central Utah. *J Sediment Petrol* 48:587–594.
5. Darragi F, Tardy Y (1987) Authigenic trioctahedral smectites controlling pH, alkalinity, silica and magnesium concentrations in alkaline lakes. *Chem Geol* 63:59–72.
6. Mees F (2001) An occurrence of lacustrine Mg-smectite in a pan of the southwestern Kalahari, Namibia. *Clay Miner* 36:547–556.
7. Meunier A (2005) in *Clays* (Springer, Berlin).
8. Banfield JF, Jones BF, Veblen DR (1991) An AEM-TEM study of weathering and diagenesis, Abert Lake, Oregon, II. Diagenetic modification of the sedimentary assemblage. *Geochim Cosmochim Acta* 55:2795–2810.
9. Bellanca A, Calvo JP, Censi P, Neri R, Pozo M (1992) Recognition of lake-level changes in Miocene lacustrine units, Madrid Basin, Spain - Evidence from facies analysis, isotope geochemistry and clay mineralogy. *Sediment Geol* 76:135–153.
10. Webster DM, Jones BF (1994) in *Sedimentology and Geochemistry of Modern and Ancient Saline Lakes*, eds Renaut RW, Last WM (SEPM, Tulsa, Okla) Special Publication 50, pp 159–172.
11. Birsoy R (2002) Formation of sepiolite-palygorskite and related minerals from solution. *Clays Clay Miner* 50:736–745.
12. Vernhet E, Heubeck C, Zhu MY, Zhang JM (2006), Large-scale slope instability at the southern margin of the Ediacaran Yangtze platform (Hunan province, central China). *Precambrian Res* 148:32–44.
13. Vernhet E (2007) Paleobathymetric influence on the deveolpment of the late Ediacaran Yangtze platform (Hubei, Hunan, and Guizhou provinces, China). *Sediment Geol* 197:29–46.
14. Jiang GQ, Sohl LE, Christie-Blick N (2003) Neoproterozoic stratigraphic comparison of the Lesser Himalaya (India) and Yangtze block (south China): Paleogeographic implications. *Geology* 31:917–920.
15. Jiang GQ, Kennedy MJ, Christie-Blick N, Wu HC, Zhang SH (2006) Stratigraphy, sedimentary structures, and textures of the late neoproterozoic doushantuo cap carbonate in south China. *J Sediment Res* 76:978–995.
16. Raiswell R, Buckley F, Berner RA, Anderson TF (1988) Degree of pyritization of iron as a paleoenvironmental indicator of bottom-water oxygenation. *J Sediment Petrol* 58:812–819.
17. Van Denburgh AS (1975) in *Solute Balance at Abert and Summer Lake, South-central Oregon.* (US Geological Survey, Washington), Professional paper 502-C.
18. Yuretich RF, Cerling TE (1983) Hydrogeochemistry of Lake Turkana, Kenya: Mass balance and mineral reactions in an alkaline lake. *Geochim Cosmochim Acta* 47:1099–1109.
19. Hay RL, et al. (1991) Clay mineral diagenesis in core Km-3 of Searles Lake, California. *Clays Clay Miner* 39:84–96.
20. Hover VC, Walter LM, Peacor DR, Martini AM (1999) Mg-smectite authigenesis in a marine evaporative environment, Salina Ometepec, Baja California. *Clays Clay Miner* 47:252–268.
21. Martini AM, Walter LM, Lyons TW, Hover VC, Hansen J (2002) Significance of early-diagenetic water-rock interactions in a modern marine siliciclastic/evaporite environment: Salina Ometepec, Baja California. *Geol Soc Am Bull* 114:1055–1069.
22. Zeebe RE, Wolf-Gladrow D (2001) in *CO_2 in Seawater: Equilibrium, Kinetics, Isotopes* (Amsterdam, Elsevier).
23. Tréguer P, et al. (1995) The silica balance in the world ocean: A reestimate. *Science* 268:375–379.
24. Khoury HN, Eberl DD, Jones BF (1982) Origin of magnesium clays from the Amargosa Desert, Nevada. *Clays Clay Miner* 30:327–336.
25. Eberl DD, Jones BF, Khoury HN (1982) Mixed-layer kerolite stevensite from the Amargosa Desert, Nevada. *Clays Clay Miner* 30:321–326.
26. Hay RL, Kyser TK (2001) Chemical sedimentology and paleoenvironmental history of Lake Olduvai, a Pliocene lake in northern Tanzania. *Geol Soc Am Bull* 113:1505–1521.
27. Hover VC, Ashley GM (2003) Geochemical signatures of paleodepositional and diagenetic environments: A STEM/AEM study of authigenic clay minerals from an arid rift basin, Olduvai Gorge, Tanzania. *Clays Clay Miner* 51:231–251.
28. Sandler A, Nathan Y, Eshet Y, Raab M (2001) Diagenesis of trioctahedral clays Miocene to Pleistocene in a sedimentary-magmatic sequence in the Dead Sea Rift, Israel. *Clay Miner* 36:29–47.
29. Dyni JR (1976) in *Trioctahedral smectite in the Green River Formation, Duchesne County, Utah* (US Geological Survey, Washington), Professional paper 967.
30. Setti M, Marinoni L, Lopez-Galindo A (2004) Mineralogical and geochemical characteristics (major, minor, trace elements and REE) of detrital and authigenic clay minerals in a Cenozoic sequence from Ross Sea, Antarctica. *Clay Miner* 39:405–421.
31. April RH (1981) Clay petrology of the upper triassic-lower Jurassic terrestrial strata of the Newark Supergroup, Connecticut-Valley, USA. *Sediment Geol* 29:283–307.
32. April RH (1981) Trioctahedral smectite and interstratified chlorite-smectite in Jurassic strata of the Connecticut Valley. *Clays Clay Miner* 29:31–39.
33. Bodine MW, Madsen BM (1987) Mixed-layer chlorite/smectite from a Pennsylvanian evaporite cycle, Grand County, Utah *in* Proceedings of the International clay conference, Denver, CO, United States 8:85–93.
34. Hillier S (1993) Origin, diagenesis, and mineralogy of chlorite minerals in Devonian lacustrine mudrocks, Orcadian Basin, Scotland. *Clays Clay Miner* 41:240–259.

35. Tuttle ML, Dean WE, Parduhn NL (1983) in *Geochemistry of Oil Shales*, eds Miknis FP, McKay JF (American Chemical Society, Washington DC), ACS Symp Ser 230, pp 249–267.
36. Bishop JL, et al. (2001) Mineralogical and geochemical analysis of Antarctic lake sediments: A study of reflectance and Mössbauer spectroscopy and C, N and S isotopes with applications for remote sensing on Mars. *Geochim Cosmochim Acta* 65:2875–2897.
37. Kríbek B, et al. (1998) Geochemistry of Miocene lacustrine sediments from the Sokolov Coal Basin (Czech Republic). *Int J Coal Geol* 37:207–233.
38. Schaller T, Christoph Moor H, Wehrli B (1997) Sedimentary profiles of Fe, Mn, V, Cr, As and Mo as indicators of benthic redox conditions in Baldeggersee. *Aquat Sci* 59:345–361.
39. Brumsack HJ (2006) The trace metal content of recent organic carbon-rich sediments; implications for Cretaceous black shale formation. *Palaeogeogr Palaeoclimatol Palaeoecol* 232:344–361.
40. Quinby-Hunt MS, Wilde P, Orth CJ, Berry WBH (1989) in *Metalliferous Black Shales and Related Ore Deposits*, eds Grauch RI, Huyck HLO (US Geological Survey, Denver, CO) US Geol Surv Circ 1037, pp 8–15.
41. Algeo TJ (2004) Can marine anoxic events draw down the trace element inventory of seawater? *Geology* 32:477–478.
42. Scott C, et al. (2008) Tracing stepwise oxygenation of the Proterozoic ocean. *Nature* 452:456–459.

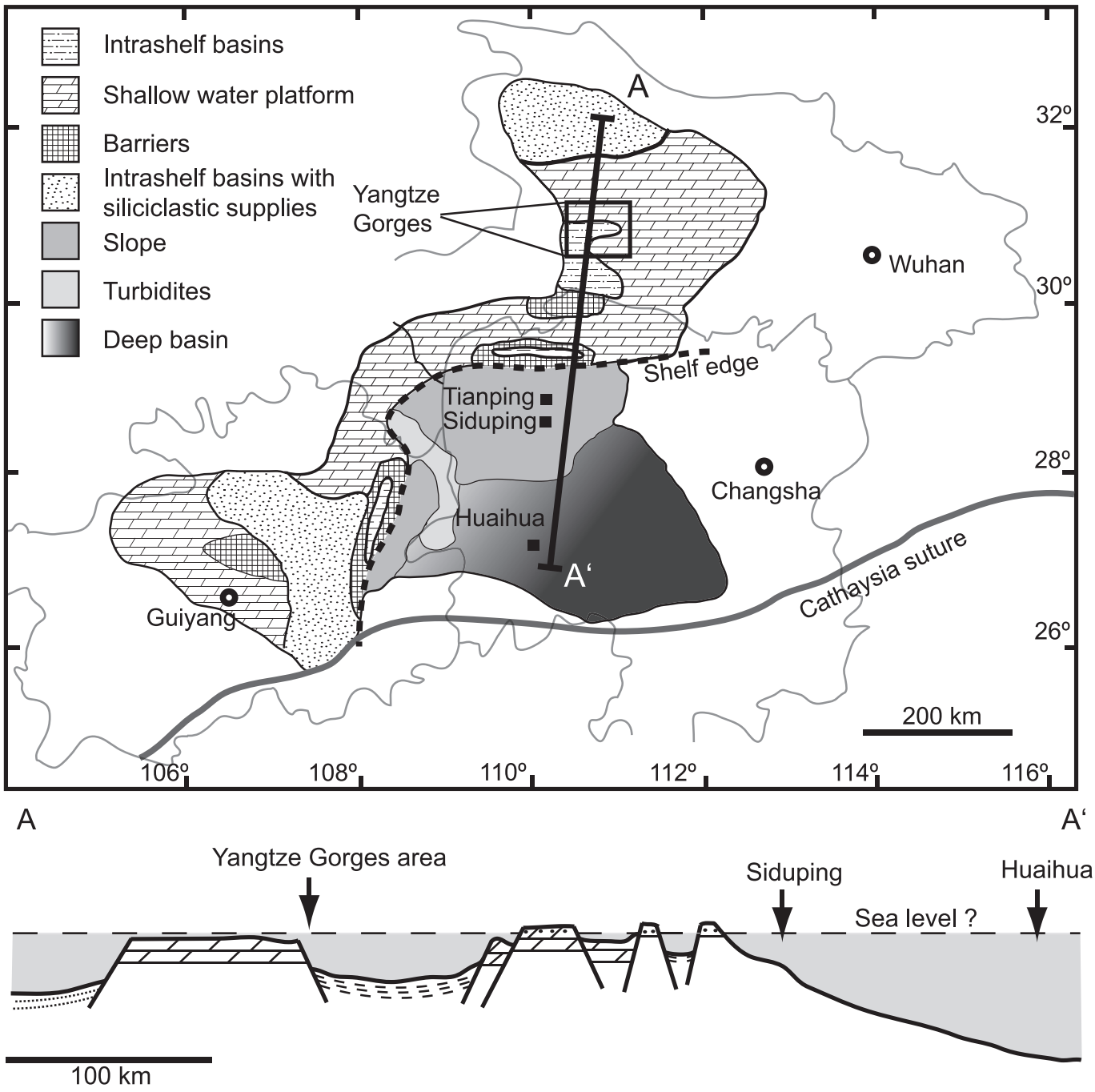

Fig. S1. Paleogeographic reconstruction of the SE margin of the Yangtze block during deposition of the Doushantuo Formation, showing the locations of the sections collected and analyzed in the Yangtze Gorges area, Siduping and Huaihua. This reconstruction, from work by Vernhet (12, 13), with a series of fault bound basins and horsts, is based on observations of rapid lateral variations in thickness and lithology of the Doushantuo Formation and widespread evidence of gravity induced sediment instability. Jiang et al. (14, 15) have a different model, with a rimmed carbonate platform forming on a passive margin.

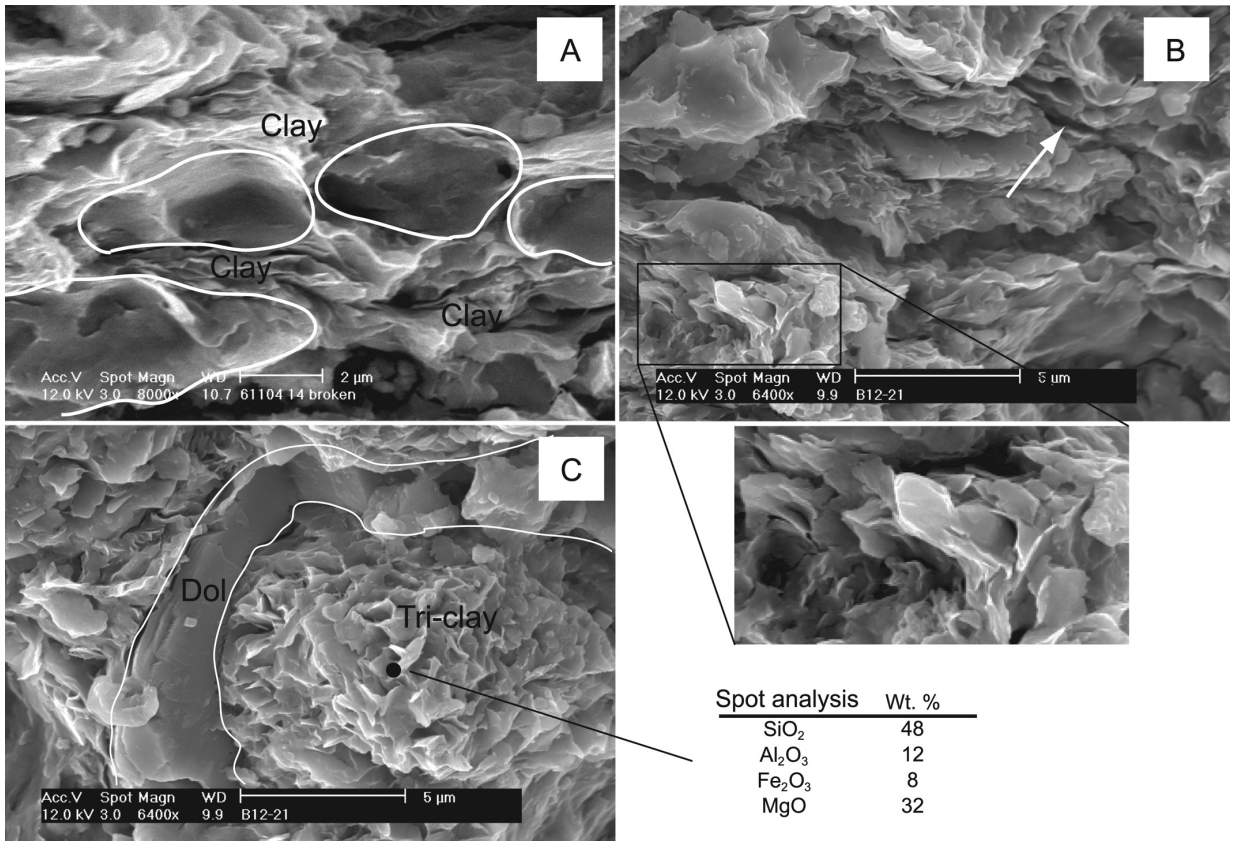

Fig. S2. SEM photomicrographs of member 2 mudstones. Dol, dolomite; Tri clay, trioctahedral clay. (*A*) Subparallel clay layers between larger grains. (*B*) White arrow and enlarged box highlight examples of randomly orientated clay aggregates. (*C*) Sphere of authigenic clay, either saponite or corrensite as indicated by elemental analysis. Clay sphere has an overgrowth of platy dolomite.

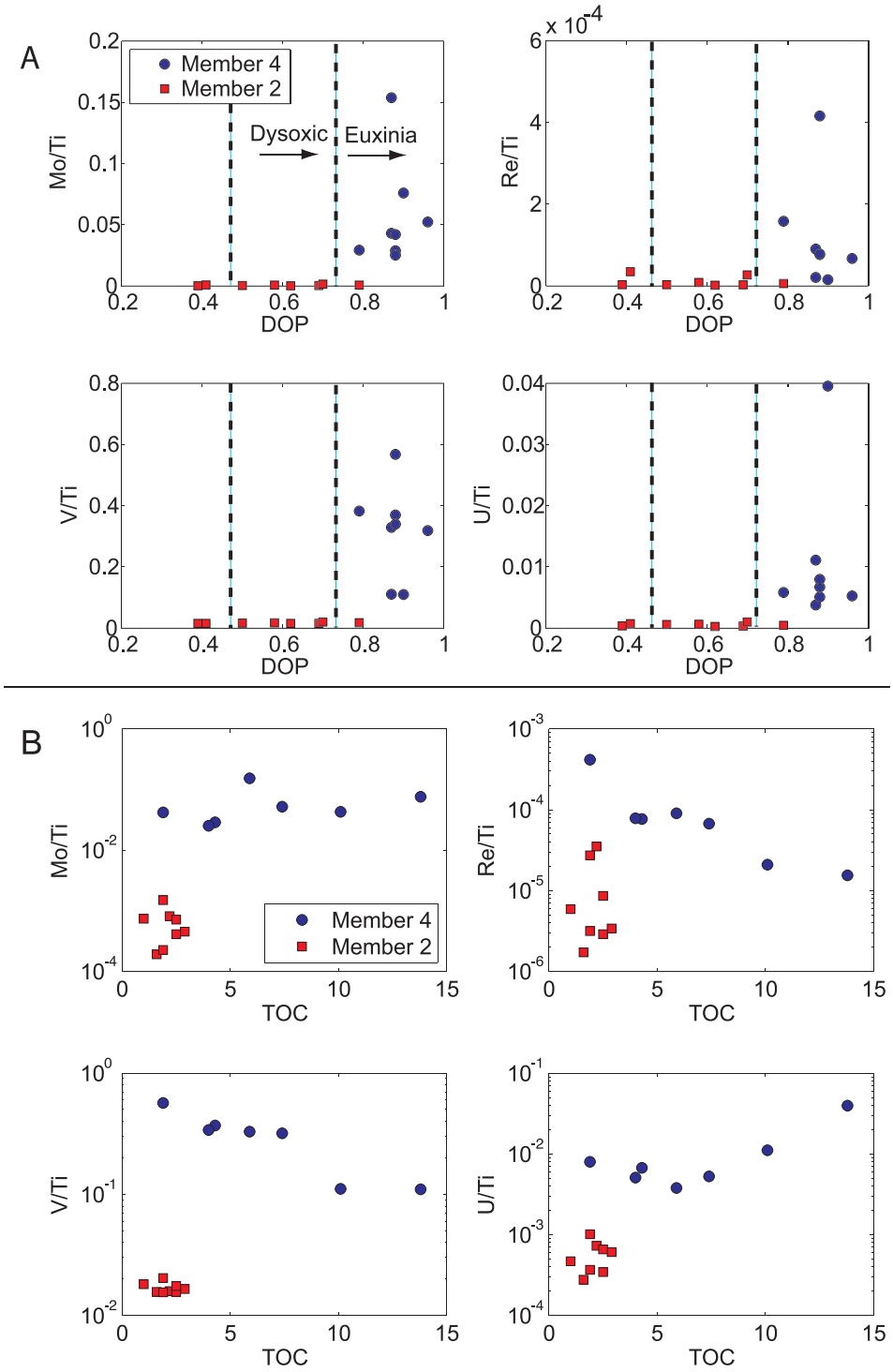

Fig. S3. Distribution of redox-sensitive elements in members 2 and 4 of the Doushantuo Formation in the Yangtze Gorges region. (*A*) Plots of redox sensitive element concentrations (Mo, Re, V, and U—normalized to Ti to correct for differences in sedimentation rate) vs. degree of pyritization (DOP) as an independent measure of redox conditions. DOP values >0.75 (to the right of the dotted line) indicate anoxic bottom water which was intermittently sulfidic (euxinic) (16). DOP values >0.45 indicate dysoxic conditions. Oxygen depletion in the water column is expected to promote enrichments in redox sensitive elements. Despite suitable conditions, elemental enrichments are absent in member 2. (*B*) Plots of redox sensitive element concentrations (Mo, Re, V, and U) normalized to Ti vs. total organic carbon (TOC) as weight percent. Covariation between TOC and elemental abundance in member 4 shales suggest that sedimentary organic content influences elemental enrichment. However, member 2 shales have normalized abundances 1 to 2 orders of magnitude lower than member 4 shales with similar organic content. Panel (*A*) shows that this difference is not the result of changing bottom water redox conditions. We suggest that elemental abundance is a function of depositional environment. In nonmarine settings enrichment is limited by supply from local catchment. Marine shales draw from a significantly larger reservoir—the global ocean. Note logarithmic scale of *y* axis.

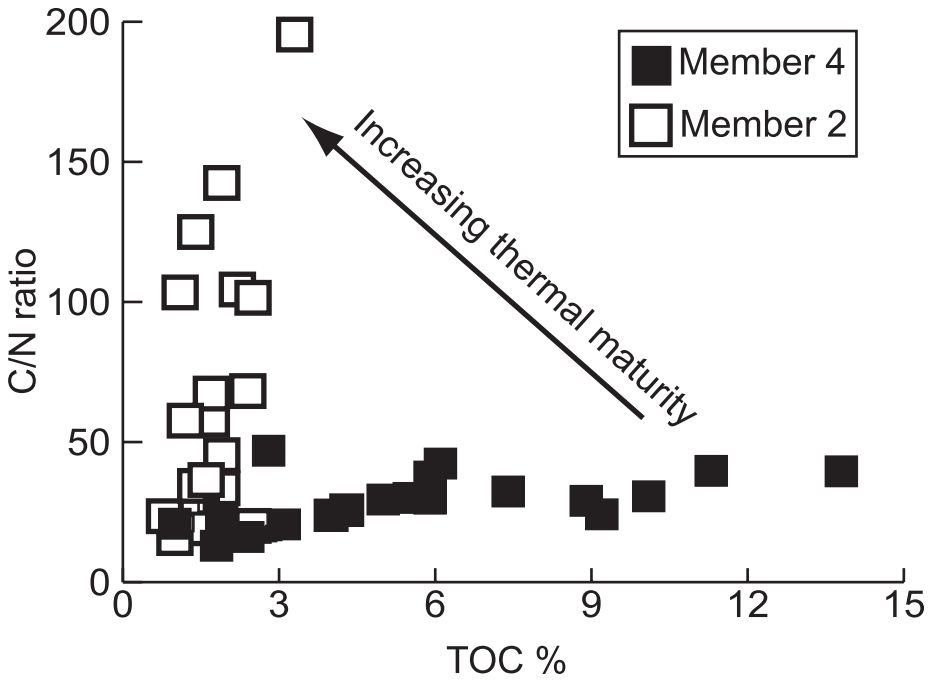

Fig. S4. Plot of C/N ratios vs. TOC for members 2 and 4 mudstones from Jiulongwan and Huajipo. The expected change in C/N ratio associated with increasing thermal maturation is shown. However, the clay mineralogy of ash beds indicates that members 2 and 4 are thermally equivalent so this does not account for differences in C/N ratios.

Table S1. Elemental analysis of clay fractions from representative samples (A), corrected elemental composition of saponite-rich samples accounting for the phosphate and K-feldspar content (B), and unit formulae of saponites set to 22 charges calculated using the corrected compositions of saponites (C)

	Mem. 2 61104-21 $< 0.2\ \mu m$	Mem. 2 61104-41A $< 0.2\ \mu m$	Mem. 2 61805-20 $< 0.5\ \mu m$	Mem. 2 61104-30 $< 0.2\ \mu m$	Mem. 2 61805-8 $< 0.5\ \mu m$	Mem. 1 61104-2 $< 0.5\ \mu m$	Mem. 2 61805-2 $< 0.5\ \mu m$	Mem. 4 61905-1 $< 0.5\ \mu m$	Mem. 4 61905-13 $< 0.5\ \mu m$
A. Clay mineralogy	Saponite	Saponite	Saponite + minor corrensite	Corrensite	Corrensite + minor chlorite	Chlorite	I/S + chlorite	I/S	I/S
SiO_2	54.91	52.97	65.57	51.16	59.80	67.57	58.50	70.82	66.62
Al_2O_3	9.49	7.71	8.21	13.68	12.70	13.09	19.00	18.33	19.93
TiO_2	0.78		0.61	0.75	0.90	1.75	1.40	0.87	0.91
Fe_2O_3	4.34	2.76	2.57	3.04	4.00	2.01	3.70	1.16	1.51
MgO	26.32	26.01	16.36	29.52	20.80	13.32	12.50	2.02	3.33
CaO	0.74	3.88	1.55	0.67		0.45			1.06
Na_2O	2.82	2.25	2.06	1.49	1.10	0.27	1.20	0.51	0.87
K_2O	0.60		1.25		0.70	1.55	3.70	6.30	4.60
P_2O_5		4.27	1.84		0.00				1.17
Total	100	99.85	100.02	100.31	100	100.01	100	100.01	100
B.									
SiO_2	54.55	57.76							
Al_2O_3	9.17	8.41							
TiO_2	0.81	0							
Fe_2O_3	4.50	3.01							
MgO	27.29	28.36							
CaO	0.77	0							
Na_2O	2.92	2.45							
K_2O	0	0							
P_2O_5	0	0							
Total	100	100							
C. Tetrahedral									
Si	3.468	3.584							
Al	0.532	0.416							
Sum	4.000	4.000							
Octahedral									
Al	0.155	0.198							
Mg	2.585	2.622							
Fe^{2+}	0.215	0.141							
Sum	2.956	2.961							
Interlayer									
Ca	0.052	0							
Na	0.360	0.295							
K	0	0							
Charge									
Tetrahedral	−0.532	−0.416							
Octahedral	0.155	0.198							
Total	−0.377	−0.218							
Interlayer	0.465	0.295							

Several samples contain a calcium phosphate phase, K-feldspar and silica as contamination. To make the corrections, all K was assumed to be in K-feldspar and all P and Ca in apatite. All Fe is assumed to be in the octahedral layer and ferrous, silica contamination is not accounted for. The tetrahedral, octahedral, and interlayer charge were calculated separately to highlight the potential misfit (which is low).

Table S2. Mineralogical composition (wt %) of representative samples from the Nantuo (boldface), Doushantuo (black), and Dengying (italic) Formations in the Yangtze Gorges as well as Doushantuo Formation (black) and Nantuo Formation samples from basin section at Siduping

Sample	Sample height, m	Saponite + corrensite	Chlorite	Illite	Quartz	K-feldspar	Plagioclase	Dolomite	Calcite
Yangtze Gorges									
61304 100	*184*	*0*	*0*	*0*	*10*	*0*	*0*	*90*	*0*
61905_13	180	0	0	26	32	18	0	23	1
61905_1	175	0	0	29	36	19	0	16	0
62005_9	174	0	0	2	5	0	0	12	81
62005_8	170	0	0	4	4	0	0	26	66
61304_73	120	0	0	4	3	0	0	93	
61304_63a	105	0	0	0	12	0	0	88	0
61805_21	81	28	0	0	16	4	0	52	0
61805_20	80	24	0	0	26	4	0	46	0
61805_18	70	13	0	0	22	4	0	61	0
61805_15	63	26	0	0	15	5	2	52	0
61805_14	33	21	0	1	31	24	11	13	0
61104_30	18	7	0	0	8	0	0	42	42
61805_8	15	13	11	0	38	3	0	32	3
61104_27	13	30	0	0	27	7	9	26	0
61104_21	10.5	10	0	0	30	5	0	55	0
62205_3	9.6	0	0	69	22	9	0	0	0
61805_2	9.5	0	13	43	32	0	0	9	3
61104_14	8	6	0	0	38	0	0	56	0
61105_11	6	23	0	0	19	0	8	50	0
61104_7	4.5	10	0	0	20	0	0	70	0
61104 _5	1	2	0	0	11	0	0	44	44
61104_3	**−5**	**0**	**13**	**28**	**45**	**0**	**13**	**0**	**2**
Basin									
61704_TB16	51	0	18	0	33	11	0	38	0
61704_TB14	49	0	11	0	33	6	0	50	0
61704_TB15	46	0	10	0	17	3	0	70	0
61704_TB13	38	0	20	12	27	39	0	2	0
61704_TB11	22	0	0	26	31	41	0	2	0
61704_TB10	16	0	0	22	39	37	0	2	0
61704_TB5	12	0	0	24	34	40	0	2	0
61704_TB6	11	0	0	32	35	33	0	0	0
61704_TB7	5	0	0	12	9	0	0	80	0
61704_TB2	**−0.5**	**0**	**10**	**23**	**41**	**21**	**0**	**0**	**5**

Sample collection sites:
61104_1 to 21 Huajipo section 2 at 30°46′53.2″N, 111°02′05.4″E.
61104_27, 30 and 62005 Huajipo section 1 at 30°47′09.5″N, 111°02′05.5″E.
61304 Sixi section 30°45′25.8″N, 110°55′51.0″E.
61805 and 61905 Jiulongwan Section 30°48′38.0″N 110°03′27.0″E.
62205 Jiuqunao Section 30°53′04.4″N, 110°52′36.1″E.
61704 Siduping section 28°55′05.9″N, 110°27′03.1″E.

Table S3. Comparison of trace element concentrations in anoxic lacustrine and anoxic marine sediments with the Doushantuo Formation

Anoxic lacustrine sediments	Mo, ppm	Re, ppb	V, ppm	U, ppm	Ref.
Green River Fm, core 01-a	22		83		35
Green River Fm, core cr-2	18		78		35
Antarctic dry lakes	<4		113	<5	36
Sokolov Fm	2		299		37
Lake Baldeggersee	5		74		38
Anoxic marine sediments					
Black Sea Unit 1	51	34	100	10.9	39
Black Sea Unit 2	117	54	196	14.8	39
Average black shale (Cambrian to Jurassic)	65		500		40
Peruvian margin (modern)	42	49	152	3.7	39
Namibian mud lens (modern)	40	27	138	10.5	39
Mediterranean sapropels	105	295	518	15.5	39
Average Devonian black shale	170		500	15	41
Average Cretaceous/Tertiary black shale	316	210	1016	28	33
Average black shale 2 Ga to 600 Ma	24				42
Doushantuo					
Member 2 Yangtze Gorges ($n = 8$)	2.5	36	72	2.2	
Member 4 Yangtze Gorges ($n = 8$)	150	317	613	29	
Basin shales ($n = 10$)*	30		329		

Data from the Yangtze Gorges area are also shown in Fig. S3. Basin shale data come from Siduping and Huaihua sections.

Table S4. Ancient occurrences of trioctahedral smectite

Location	Age + setting	Clay minerals	Associated minerals	Chemical conditions	Ref(s).
Double Lakes Fm, West Texas	Saline lake (Quaternary)	Mg-smectite (dioctahedral) sepiolite, palygorskite. Clay content 20–60%.	Calcite, dolomite, feldspars and quartz. Traces of gypsum and other sulfate minerals	Most saline during Mg-smectite deposition	10
Amargosa desert, California	Saline lake (Pliocene-Pleistocene)	Sepiolite, kerolite/ stevensite Clay content up to 70%, average ~30%)	Calcite and dolomite + detrital mica, feldspar, quartz - altered to chlorite and sericite	pH above 9 inferred for trioct-smectite stages	24, 25
Olduvai Gorge, Tanzania rift zone	Saline-alkaline lake (Plio-Pleistocene)	Trioctahedral smectite (stevensite), illite	Celadonite, zeolites, K-feldspars, calcite, pseudomorphs of evaporative minerals	pH 9.5–10 inferred from Magadi-type chert nodules	26, 27
South of Sea of Galilee, Dead Sea Rift zone	Evaporative lake (Miocene to Pleistocene)	Saponite, corrensite, chlorite (diagenetic series), only occurs at 600-m depth (clays 30–60%)	I-S, palygorskite, illite, kaolinite, talc, calcite, dolomite, quartz, feldspar, halite, gypsum	Saponite favored in reducing alkaline conditions	28
Madrid Basin, Spain	Continental basin - saline to freshwater lake system (Miocene)	Saponite, sepiolite, palygorskite, mainly in evaporative stage, dioctahedral smectite, illite and kaolinite in freshwater stage.	Abundant calcite and dolomite, chert beds and nodules, detrital quartz, feldsparand mica, rare gypsum.	Saline conditions	9
Green River Fm, Utah	Saline lake system (Eocene)	Trioctahedral smectite, minor mixed-layer illite and chlorite	Quartz, K-feldspar, mixed calcite and dolomite	Near-shore lacustrine, mildly reducing, moderately saline	29
Ross Sea, Antarctica	Oligocene to early Eocene Hydrothermal (low temp) altered marine volcanoclastic detritus	up to ~50% clay, saponite-badeillite series normally 100% of clay content.	No other authigenic minerals: chlorite and illite and di-smectite in upper part of core that is not altered. Mainly quartz, feldspar, trace calcite, pyroxene, amphibole	Low temperature hydrothermal alteration (<150°C)	30
East Berlin Fm, Connecticut Valley	Lacustrine (Upper Triassic/Lower Jurassic)	Trioctahedral smectite, corrensite, illite, chlorite + I/S	Quartz, plagioclase, calcite, dolomite	Alkaline conditions	31, 32
Paradox Basin, South-east Utah	Marine evaporite sequence (Middle Pennsylvanian)	Interstratified chlorite/tri-smectite (from corrensite to discrete chlorite) + detrital(?) illite	Anhydrate, halite dolomite, quartz	Evaporitic basin	33
Orcadian Basin, Scotland	Devonian lacustrine	Corrensite to chlorite with mixtures of discrete corrensite and chlorite	Inverse relationship between tri-clay and dolomite abundance indicate late diagenetic conversion of 2:1 di-clays	Purely diagenetic phase	34

Table S5. Chemical conditions in recent sedimentary settings where trioctahedral smectites form

Location	Mineralogy	Chemistry			Ref(s).
		Mg, ppm	Si, ppm	pH	
Abert Lake, Orogen	Mg-smectites of variable composition, interpreted as interstratified dioctahedral precursors and neoformed K-stevensite, minor kaolinite and mica, calcite, Na-carbonate, halite, feldspars, quartz.	0.6	144	9.6	8, 17
Lake Yoa, Chad	Stevensite mixed with aragonite forms ooids. Minor kaolinite + dolomite, Na-carbonates/sulfates and halite.	≈2.8	34 to 304	9.3 to 9.9	5
Lake Turkana	Presence of Mg-silicate phase (sepiolite or tri-smectite) inferred based on mass balance considerations (sink for Mg and Si). Some increased smectite crystallinity observed lakeward supports this. Mg-silicates estimated to make up to 4% of sediment.	2.3 (ave.)	19.8 (ave.)	9.2 (ave.)	18
Searles Lake, California	Trioctahedral Mg-smectite, Fe-illite, K-feldspar, analcime, kaolinite, chlorite, evaporite minerals and quartz.	?	?	pH 9 to 10 measured from pore fluids	19
Salina Ometepec, Baja California	Neoformed and transformed saponite (from dioctahedral smectite) with variable composition. Other minerals include kaolinite and minor illite, quartz, gypsum and halite—little/no carbonate.	8361 to 16941	1.1 to 3.1	6 to 8	20, 21
Modern ocean	Dominantly detrital 2:1 and 1:1 Al-clays	1318	≈4.5	7.8 to 8.2	22, 23